Atmospheric Environment 73 (2013) 103–111

Contents lists available at SciVerse ScienceDirect

Atmospheric Environment

journal homepage: www.elsevier.com/locate/atmosenv

Numerical study of the urban heat island over Athens (Greece) with the WRF model

Theodore M. Giannaros [a,*], Dimitrios Melas [a], Ioannis A. Daglis [b], Iphigenia Keramitsoglou [b], Konstantinos Kourtidis [c]

[a] Laboratory of Atmospheric Physics, Aristotle University of Thessaloniki, PO Box 149, 54124 Thessaloniki, Greece
[b] National Observatory of Athens, Institute for Astronomy, Astrophysics, Space Applications and Remote Sensing, Vas. Pavlou & Metaxa, 15236 Athens, Greece
[c] Laboratory of Atmospheric Pollution and Pollution Control Engineering of Atmospheric Pollutants, Department of Environmental Engineering, Democritus University of Thrace, 67100 Xanthi, Greece

HIGHLIGHTS

- The urban heat island in Athens, Greece, is studied with a meteorological model.
- The model shows a global satisfactory performance.
- The canopy-layer heat island is strongest during the night (up to 4 °C).
- The city surface is cooler than its surroundings during the day.
- The assimilation of skin temperature data slightly improves model performance.

ARTICLE INFO

Article history:
Received 17 October 2012
Received in revised form
13 December 2012
Accepted 27 February 2013

Keywords:
Urban heat island
Numerical modeling
Remote sensing
Observations
Athens
Data assimilation

ABSTRACT

In this study, the Weather Research and Forecasting (WRF) model coupled with the Noah land surface model was tested over the city of Athens, Greece, during two selected days. Model results were compared against observations, revealing a satisfactory performance of the modeling system. According to the numerical simulation, the city of Athens exhibits higher air temperatures than its surroundings during the night (>4 °C), whereas the temperature contrast is less evident in early morning and mid-day hours. The minimum and maximum intensity of the canopy-layer heat island were found to occur in early morning and during the night, respectively. The simulations, in agreement with concurrent observations, showed that the intensity of the canopy-layer heat island has a typical diurnal cycle, characterized by high nighttime values, an abrupt decrease following sunrise, and an increase following sunset. The examination of the spatial patterns of the land surface temperature revealed the existence of a surface urban heat sink during the day. In the nighttime, the city surface temperature was found to be higher than its surroundings. Finally, a simple data assimilation algorithm for satellite-retrieved land surface temperature was evaluated. The ingestion of the land surface temperature data into the model resulted to a small reduction in the temperature bias, generally less than 0.2 °C, which was only evident during the first 4–5 h following the assimilation.

1. Introduction

Urbanization induces significant changes in land surface properties that, in turn, modify the surface energy balance. The well-documented urban heat island (UHI), characterized by the excess warmth of urban areas compared to the surrounding non-urbanized areas, is one prominent urban effect that influences air quality (e.g. Rosenfeld et al., 1998), energy consumption (e.g. Konopacki and Akbari, 2002), heat-related mortality (e.g. Conti et al., 2005) and local- and regional-scale atmospheric circulations (e.g. Miao et al., 2009). In addition, although heat islands in themselves do not influence global temperatures (Houghton et al., 2001), they do have an impact on local temperatures used for assessing climate change (Van Wevenberg et al., 2008).

Heat islands develop primarily due to differences in the surface energy budget (SEB) of urban and rural areas (Oke, 1982). During the day, urban areas store more heat than do rural areas due to the

* Corresponding author. Tel.: +30 2310 998183; fax: +30 2310 998090.
E-mail address: thgian@auth.gr (T.M. Giannaros).

1352-2310/$ – see front matter © 2013 Elsevier Ltd. All rights reserved.
http://dx.doi.org/10.1016/j.atmosenv.2013.02.055

surface enlargement provided by canyon-like geometry and the thermal properties of urban fabric. Following sunset, urban and rural temperatures begin to diverge, generating the heat island in the canopy-layer. The rural environment starts cooling quickly after sunset due to its open exposure and generally unobstructed sky view. Conversely, the cooling rate of the urban environment is significantly reduced due to the decreased sky view factor and the increased release of storage heat from the urban surfaces (Grimmond and Oke, 1995). Normally, the canopy-layer heat island persists overnight, until shortly after sunrise the daily solar radiation cycle begins and the rural area starts warming quickly.

During the past few decades, significant progress has been recorded with regards to the understanding and modeling of the complex processes that take place in the urban boundary layer (UBL), contributing to the formation of the UHI (Martilli, 2007; Masson, 2006). The development of sophisticated atmospheric models along with experimental campaigns has contributed notably towards this direction. Especially during the past decade, several parameterizations have been proposed for representing the mesoscale impact of cities (e.g. Kanda et al., 2005; Kusaka et al., 2001; Liu et al., 2006; Martilli et al., 2003).

The representation of the UHI effect in mesoscale meteorological models is thought to be of great importance for the successful simulation of the urban boundary layer (UBL) and, consequently, air pollutants' dispersion and transport. This is because the thermodynamic properties of the UBL can be significantly modified by the UHI effect. For instance, Pal et al. (2012) recently showed that the spatio-temporal variability of the boundary layer over Paris, France, is closely related to the intensity of the UHI. Martilli et al. (2003) also concluded that the parameterization of the thermodynamic impact of cities, induced by the heat island formation mechanism, can significantly modify pollutants' distribution.

Land surface temperature (LST) lies at the heart of the SEB and is considered to be an important variable in meteorological models. It influences the sensible and latent heat fluxes, through which it affects the development of the UHI. Accurate LST specification is therefore significant for improving the accuracy of heat island simulations. In the past few years, satellite-retrieved LST data have been widely assimilated into weather and climate models to either improve the initialization of soil moisture (e.g. Lakshmi, 2000) or account for the overall model biases (e.g. Bosilovich et al., 2007).

Athens is the largest city of Greece, both in terms of population and area extend. Although the UHI in Athens is well documented since decades (Katsoulis, 1987), the number of relevant modeling studies is rather limited. Several meteorological studies over the greater Athens area (GAA) have been conducted in the past, but mostly focusing on either air quality (e.g. Kotroni et al., 1999; Moussiopoulos et al., 1995) or local-scale atmospheric circulations (e.g. Grossi et al., 2000; Melas et al., 1998a,b). Only the numerical studies of Martilli et al. (2003) and Dandou et al. (2005, 2009) focused on the urban effect of Athens, by incorporating explicitly modified boundary layer parameterizations.

In the summer of 2009, the THERMOPOLIS2009 campaign (Daglis et al., 2010b) took place in Athens. The campaign was funded by the European Space Agency (ESA) as part of the "Urban Heat Islands and Urban Thermography" (hereafter "the UHI project") Data User Element (DUE) project. One of the key objectives of the campaign was to combine concurrently acquired airborne, spaceborne and ground-based measurements to generate spectrally and geometrically representative datasets with the purpose to address the observational requirements of the UHI project (Daglis et al., 2010a). The spatially and temporarily rich observational dataset collected during THERMOPOLIS2009 provided us with a unique opportunity to implement and evaluate a mesoscale modeling system comprised of the numerical weather prediction (NWP) Weather Research and Forecasting (WRF) model coupled with the advanced Noah land surface model (LSM). The collected observational data were also exploited for evaluating a simple data assimilation scheme for satellite-retrieved LST data.

The present study aims to fill the gap of modeling studies focusing explicitly on the UHI effect, by combining numerical simulations and observations to investigate the spatio-temporal structure of Athens' heat island. The key objective is to examine the degree to which the WRF/Noah modeling system can capture the major features of the heat island phenomenon, which are of importance for a successful simulation of the UBL. Further, a simple data assimilation algorithm for LST is evaluated, focusing on the potential impact on air temperature simulation.

2. Data sources

2.1. Description of the study area

Athens (37°58′N, 23°43′E) is located in a small peninsula situated in the south-eastern end of the Greek mainland (Fig. 1a). The GAA covers about 450 km^2 and the urban zone sprawls across the central plain of a basin that is often referred to as the Attica Basin. The city is bound by Mount Aigaleo to the west, Mount Parnitha to the north, Mount Penteli to the north-east, Mount Hymettus to the east, and the Saronic Gulf to the south-west (Fig. 1b). The industrial zone of Athens is located in the western part of the basin (Thriassion Plain), while the Mesogeia Plain dominates in the south-east part of the peninsula (Fig. 1b).

2.2. THERMOPOLIS2009

During the period from July 15 to July 31, 2009, the THERMOPOLIS2009 campaign took place in Athens. In the frame of this campaign, a significant number of researchers and institutes were deployed in the GAA, conducting ground-based and airborne measurements. These measurements were scheduled to coincide with specific satellite overpasses (Daglis et al., 2010a,b). This section aims to describe only the part of the experimental campaign that is relevant to the present study; that is a subset of the ground-based and satellite remote sensing observations.

The locations of the ground-based measurement sites that were deployed during THERMOPOLIS2009 are shown in Fig. 1c. Table 1 summarizes the characteristics of each measurement site. Air temperature and relative humidity were measured by a network of stations operated by the Democritus University of Thrace (DUTH), the National Observatory of Athens (NOA), the Hellenic National Meteorological Service (HNMS) and the National and Technical University of Athens (NTUA).

Besides in situ observations, the campaign included remote sensing data from the Terra and Aqua satellites, both part of NASA's Earth Observing System (EOS). In particular, the campaign included data from MODIS (Moderate Resolution Imaging Spectroradiometer), a key instrument on board Terra and Aqua. MODIS has twenty infrared bands; however, only two of them are suitable for LST retrievals, namely bands 31 and 32 at 11.0 μm and 12.0 μm, respectively. The spatial resolution of these thermal infrared (TIR) bands is approximately 1 km. Two MODIS images were used for validating the model LST in this study: one acquired at 09:15 UTC and one at 20:20 UTC on July 25, 2009.

3. Numerical simulation setup and evaluation methods

3.1. Meteorological model configuration and physics

The meteorological model used in this study is the WRF-ARW (Advanced Research Weather), version 3.2 (Skamarock et al.,

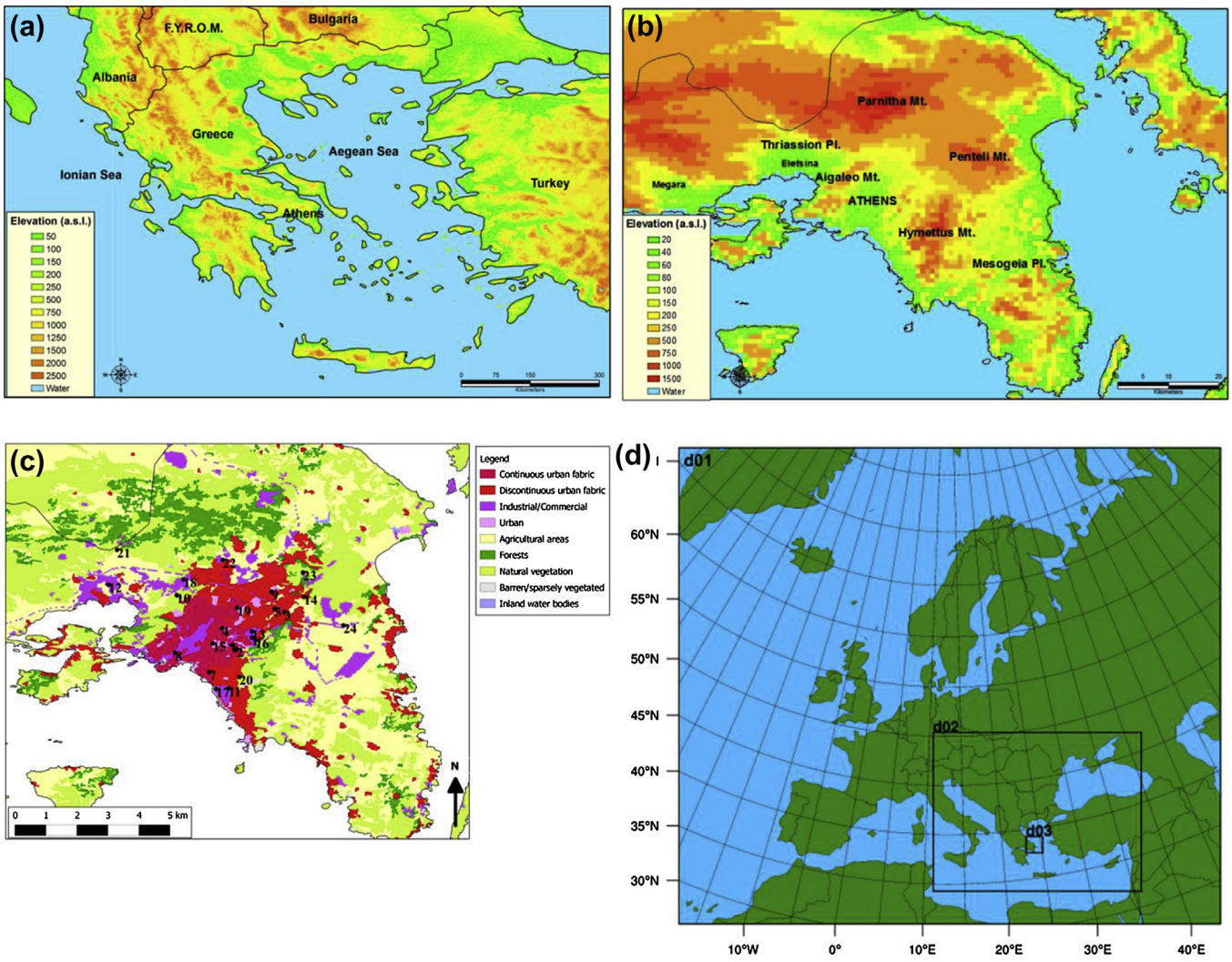

Fig. 1. (a) Topography of Greece with identification of the city of Athens. (b) Topography of GAA with identification of the major topographic features. (c) Locations of the ground-based measurement sites and land use according to CORINE2000 land cover dataset. (d) Configuration of the three 1-way nested domains for the WRF simulations (elevation is provided relative to the mean sea level).

2008). Three 1-way nested domains with horizontal grid resolutions of 30 km (d01; mesh size of 199 × 175), 10 km (d02; mesh size of 229 × 175), and 2 km (d03; mesh size of 75 × 75) were specified (Fig. 1d), of which the innermost domain (d03) focuses on the study area. All modeling domains have 33 layers in the vertical dimension. The lowest model layer is defined at approximately 10 m a.g.l., while the model top is specified at 100 hPa with radiative boundary conditions for all domains.

The simple WRF single-moment six-class scheme for microphysics (Dudhia et al., 2008; Hong et al., 2004; Lin et al., 1983) was applied in all domains, while the Kain–Fritsch scheme (Kain, 2004) was used for parameterizing cumulus convection. Shortwave radiation processes were handled using a cloud radiation scheme (Dudhia, 1989) and the Eta Geophysical Fluid Dynamics Laboratory (GFDL) scheme (Schwarzkopf and Fels, 1991) was applied for longwave radiation processes. The Yonsei University (YSU) scheme was employed for the PBL (Hong et al., 2006).

3.2. Land surface model and parameterization of urban land use

Land surface processes were parameterized using the Noah LSM (Chen and Dudhia, 2001). The latter is an advanced land surface-hydrology model, based on the coupling of the diurnally dependent Penman evaporation approach of Mahrt and Ek (1984), the multi-layer soil model of Mahrt and Pan (1984), and the primitive canopy model of Pan and Mahrt (1987). It has been extended by Chen et al. (1996) to account for the modestly complex canopy resistance approach of Jacquenim and Noilhan (1990), and by Koren et al. (1999) to include frozen ground physics. The Noah LSM has one canopy layer and four soil layers with thicknesses from top to bottom of 10, 30, 60 and 100 cm. The total soil depth equals 2 m, with the upper 1 m of soil serving as the root zone depth and the lower 1 m acting as a reservoir with gravity drainage. The key role of the Noah LSM is to provide surface sensible and latent heat fluxes, and skin temperature as lower boundary conditions to the boundary layer scheme of the WRF.

Land use and land cover were parameterized using the 30-arc-sec spatial resolution IGBP (International Geosphere–Biosphere Programme) land cover database. The latter includes 20 land use categories and is derived from up-to-date MODIS data, specifically modified by NCEP (National Centre for Environmental Predictions) for being used with the Noah LSM. Land surface properties were defined as a function of the land use category. To represent zero-order effects of the urban surface, the bulk roughness approach of

Table 1
Characteristics of the measurement sites deployed during the THERMOPOLIS2009 campaign.

ID	Name	Latitude (°N)	Longitude (°E)	Altitude (m a.s.l.[a])	Sampling height (m a.g.l.[b])	LCZ[c]
1	Dorms	37°58′54″	23°46′52″	185	5	Open midrise
2	Sirinon	37°57′46″	23°45′23″	158	5	Compact midrise
3	Thalias	38°1′21″	23°50′0″	217	5	Compact lowrise
4	Pipinou	37°59′47″	23°43′59″	101	13	Compact midrise
5	Pellis	38°1′40″	23°49′3″	211	5	Compact lowrise
6	Anaximenous	37°58′11″	23°44′56″	125	13	Compact midrise
7	Kountouriotou	37°55′34″	23°42′45″	29	8	Compact midrise
8	Serifou	37°57′25″	23°39′27″	8	3	Compact midrise
9	Papayannis	38°3′19″	23°48′46″	235	3	Open midrise
10	Nea Filadelfia	38°2′59″	23°39′36″	245	2	Sparsely built
11	Helliniko-1	37°53′59″	23°44′36″	45	2	Open midrise
12	Elefsina	38°4′1″	23°33′0″	30	2	Sparsely built
13	Academy	37°59′29″	23°46′52″	130	2	Open midrise
14	Penteli-1	38°2′50″	23°51′54″	495	2	Sparsely built
15	Thisio	37°58′19″	23°43′5″	95	2	Compact midrise
16	Zografou	37°58′38″	23°47′13″	181	2	Open midrise
17	Helliniko-2	37°53′56″	23°43′24″	6	2	Open midrise
18	Ano Liosia	38°4′36″	23°40′50″	184	2	Open midrise
19	Galatsi	38°1′46″	23°45′28″	176	2	Compact midrise
20	Ilioupoli	37°55′6″	23°45′40″	206	2	Open midrise
21	Mandra	38°7′22″	23°33′49″	258	2	Sparsely built
22	Menidi	38°6′24″	23°44′2″	210	2	Compact lowrise
23	Penteli-2	38°5′11″	23°51′49″	729	2	Open set trees
24	Pikermi	38°0′4″	23°55′43″	133	2	Sparsely built

[a] Above sea level.
[b] Above ground level.
[c] Local climate zone (Stewart and Oke, 2009a,b).

Liu et al. (2006) was adopted. More precisely: (a) the roughness length was increased from 0.5 m to 0.8 m to represent turbulence generated by roughness elements and drag from buildings, (b) the surface albedo was reduced from 0.18 to 0.15 to account for shortwave radiation trapping in the urban canyons, (c) the volumetric heat capacity and the soil thermal conductivity were set to 3.0×10^6 J m^{-3} K^{-1} and 3.24 W m^{-1} K^{-1}, respectively, to represent the large heat storage in the urban surface and the underlying surfaces, and (d) the green vegetation fraction was reduced to 0.05 to decrease evaporation over the urban surface. For the non-urban categories, the values of these properties were kept as they are (default). Liu et al. (2006) have showed that the introduction of these urban land use enhancements in the Noah LSM has a significant effect on representing urban physical processes.

3.3. Model initialization and numerical experiments

The WRF simulations were initialized using the 0.5° × 0.5° spatial resolution and 6 h temporal resolution operational atmospheric analysis surface and pressure level data of the ECMWF (European Centre for Medium-Range Weather Forecasts). The lateral boundary conditions for the d01 domain were obtained by linearly interpolating the 6-hourly ECMWF analysis data, while for the innermost d02 and d03 domains they were formed through interpolation from d01. Soil moisture and temperature data at the four layers specified in the Noah LSM were initialized from the ECMWF analyses.

In the current study, the performance of the coupled WRF/Noah modeling system was evaluated using observational data from July 24 and 25, 2009, when the highest air temperatures were observed during the THEROMOPOLIS2009 campaign. A 60 h numerical simulation was conducted starting at 1200 UTC July 23 and ending at 2300 UTC July 25, 2009, providing model output at 1 h intervals. The first 12 h of the simulation were discarded as the model's spin-up period (Kusaka et al., 2012; Miao et al., 2007; Salamanca et al., 2011), while the remaining 48 h were used for carrying out the evaluation of the modeling system.

In addition to the above numerical experiment, another one was conducted ingesting satellite-retrieved LST data into the WRF model in order to investigate the impact on the simulation of the air temperature. The data assimilation algorithm used is the one recently proposed by Zhang and Zhang (2010). It is a thermodynamically consistent soil moisture assimilation scheme driven by satellite-retrieved LST data and developed in the context of the Noah LSM. To evaluate the performance of the assimilation scheme, two 24 h numerical simulations were carried out starting at 1200 UTC July 24 and ending at 1200 UTC July 25, 2009, providing model output at 1 h intervals. One MODIS image, acquired at 1150 UTC July 24, 2009, was used for providing the scheme with the LST data and consequently correcting the model's initial soil moisture estimates for the one of the two simulations. The model setup and physics options were kept the same in both simulations to allow for comparisons.

3.4. Model evaluation

In order to evaluate the performance of the coupled WRF/Noah modeling system, the model-simulated near-surface air temperatures at 2 m a.g.l. in the 2 km spatial resolution domain were first interpolated onto the locations of the measurement sites, using bilinear interpolation. The interpolated model results were then compared with concurrent observations. Several statistical measures were computed to quantitatively evaluate the model performance, namely: (1) the mean bias error (MBE, °C), (2) the root mean squared error (RMSE, °C), (3) the index of agreement (IOA), (4) the hit rate (HR), and (5) the Pearson correlation coefficient (R). In this study, the criterion for the calculation of the HR was for model-observation agreement within 2 °C (Miao et al., 2007).

The LST output of the model was assessed against coincident satellite-retrieved LST images from MODIS on a pixel to grid-point basis, including all pixels. The assessment procedure consisted of interpretation of the thermal patterns as derived from both datasets (i.e. model and satellite). The methodology implemented for the construction of the satellite LST maps was based on the split

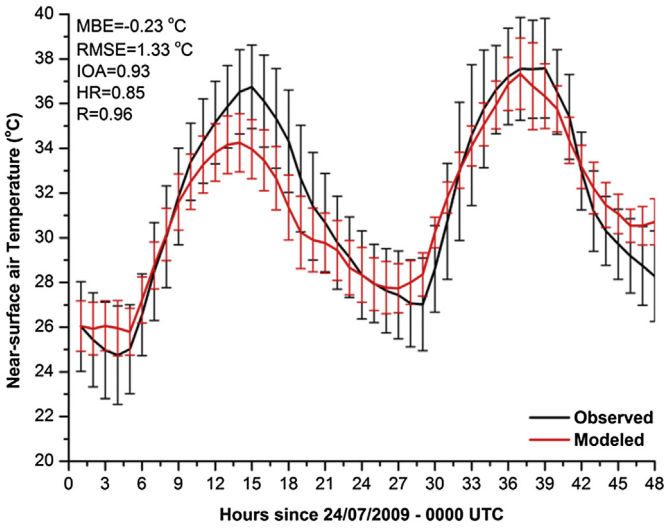

Fig. 2. Observed (solid black line) and modeled (solid red line) hourly near-surface air temperature, averaged over the 24 measurement sites from 0000 UTC July 24 to 2300 UTC July 25, 2009. The model performance metrics are presented within the plot. (For interpretation of the references to color in this figure legend, the reader is referred to the web version of this article.)

window technique (SWT) from Jimenez-Munoz and Sobrino (2008), as part of the requirements of the UHI project.

4. Results and discussion

4.1. Near-surface air temperature

Fig. 2 presents the time series of observed and modeled near-surface air temperatures, averaged over all measurement sites. Clearly, the model simulates very well the phase of the diurnal cycle (high *R* value), but underestimates its amplitude. In particular, it is evident that it underestimates the daytime maximum temperature and overestimates the nighttime minimum temperature, as also noted in previous studies (e.g. Ferretti et al., 2003; Miao et al., 2007). The underestimation of the daily maximum temperature indicates that the model underestimates either the absorbed solar radiation or the upward surface sensible heat flux, which are both considered to determine the amplitude of daytime temperatures (Miao et al., 2007). On the other hand, the overestimated daily minimum temperature provides indications that either the outgoing longwave radiation is underestimated or the upward surface heat flux is overestimated. Unfortunately, due to the lack of detailed SEB measurements during the examined period, the actual causes behind these differences cannot be specified.

Table 2 is a compilation of the computed model performance metrics for the near-surface air temperature, grouped by local climate zones (LCZ) according to Stewart and Oke (2009a,b). The "compact midrise" and "open set trees" sites showed the highest and lowest observed and modeled mean temperatures, respectively. However, the model is found to slightly underestimate the mean temperature of the most urbanized LCZ ("compact midrise"), whereas it overestimates the mean temperature of the rural LCZ ("open set trees") by about 0.5 °C. The best model performance statistics were obtained for the "compact lowrise" sites. Conversely, the worst statistics were computed for the "open midrise" sites, indicating that complex urban land use characteristics are generally harder to model. Overall, however, it can be claimed that the variation of the near-surface air temperature among the different LCZs of the study area is in good agreement with both the theory of thermal differentiation as reported by Stewart and Oke (2009a,b) and observations.

The observed and modeled spatial patterns of the near-surface air temperature in the morning (0800 LT, LT = UTC + 3), during the solar peak time (1400 LT) and during nighttime (2300 LT) were also compared (Fig. 3). The urban effect is more pronounced during the night (Fig. 3c) than during the day (Fig. 3b), while it almost disappears in the morning (Fig. 3a). This agrees with the theory of UHI formation, as stated by Oke (1982), as well as with results from previous modeling studies reporting the formation of a strong UHI effect over Athens during the night (e.g. Dandou et al., 2005; Martilli et al., 2003). As seen in Fig. 5c, significantly higher nighttime temperatures (>4 °C) are modeled and observed for the Athens metropolitan area than for the surrounding non-urbanized areas, east of the city's center (Mesogeia Pl., Fig. 1b). The diminished early morning thermal contrast is also simulated well (Fig. 3a), while during the solar peak time, the model underestimates urban temperatures by approximately 1–2 °C. The intra-urban variability of the near-surface air temperature is hardly captured by the model, mainly due to the rather coarse horizontal grid resolution of 2 km. Despite this, the sensitivity of temperature to land use and topography is generally modeled well. For instance, the relatively high daytime (Fig. 3b) and nighttime (Fig. 3c) temperatures in the western part of the domain (Thriassion Pl., Fig. 1b) are simulated quite well (|MBE| ∼ 1.5 °C). Additionally, the temperature contrast between the Attica Basin and the surrounding mountains (Fig. 1b) is reproduced well.

At this point it is worth mentioning that despite its simplicity, the adopted modeling approach shows good adequacy in simulating air temperature. The presented model evaluation results are comparable to the ones reported in previous modeling studies, employing higher-order schemes for parameterizing the urban surface (e.g. Martilli et al., 2003). This could be due to the lack of detailed urban morphology data that forces the higher-order schemes to make more general assumptions at the cost of their accuracy.

4.2. Canopy-layer urban heat island

The canopy-layer UHI is defined as the urban/rural temperature contrast observed in the urban canopy, extending from the ground up to the mean roof level (Oke, 1982). Since the present study considers

Table 2
Comparison between the observed and modeled hourly near-surface air temperatures averaged over the different local climate zones of the study area from 0000 UTC July 24 to 2300 UTC July 25, 2009.

LCZ	N_Stn[a]	Mean		St. dev.		MBE	RMSE	IOA	HR	*R*
		Obs	Mod	Obs	Mod					
Compact midrise	7	32.46	31.88	3.69	3.09	−0.58	1.35	0.92	0.85	0.95
Compact lowrise	3	31.63	31.36	4.29	3.72	−0.27	1.29	0.95	0.85	0.96
Open midrise	8	31.12	31.06	4.33	3.10	−0.06	1.85	0.88	0.69	0.93
Sparsely built	5	31.20	31.05	4.09	3.47	−0.15	1.50	0.92	0.79	0.93
Open set trees	1	28.73	29.28	4.20	3.64	0.55	1.67	0.91	0.71	0.93

[a] N_Stn: number of stations in each LCZ.

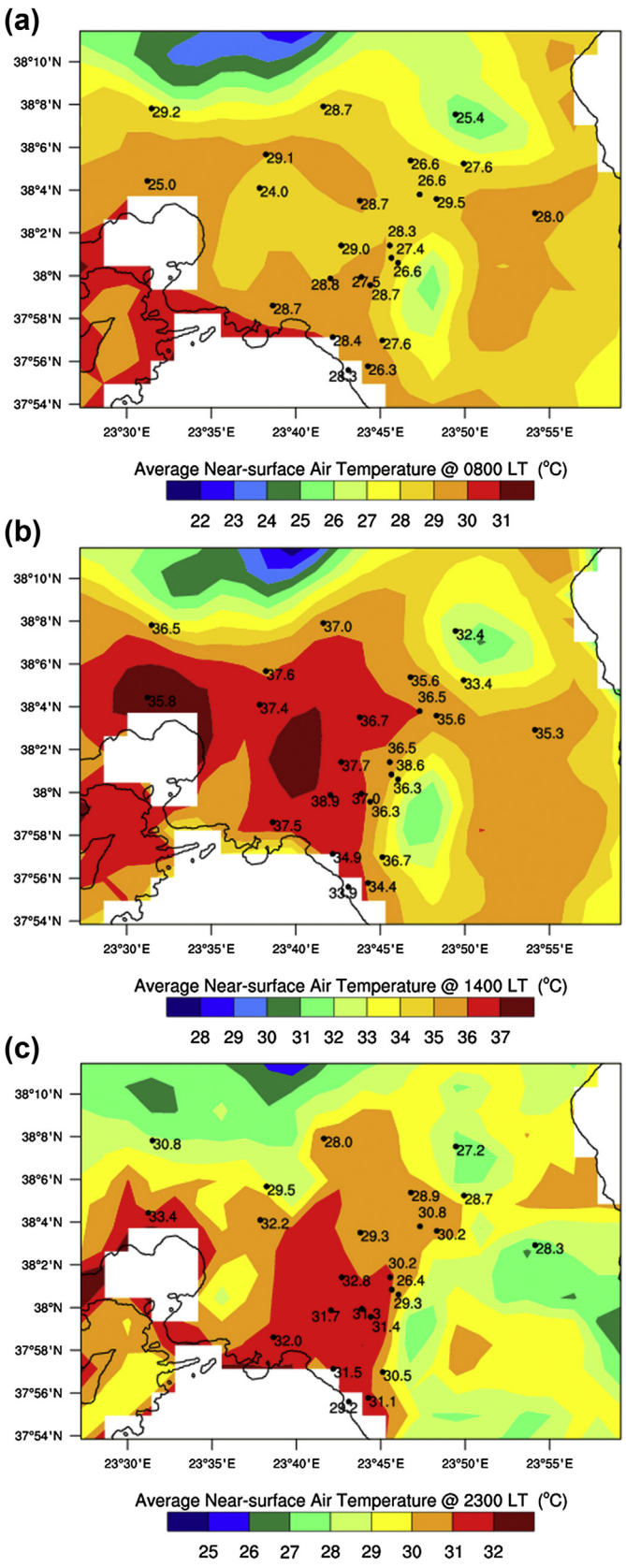

Fig. 3. Modeled spatial distribution of the near-surface air temperature (a) in the morning at 0800 LT, (b) in the daytime at 1400 LT, and (c) in the nighttime at 2300 LT. Concurrent observations are denoted by numbers.

air temperature measurements conducted within this layer, this section presents an analysis of the model's performance with respect to the simulation of the canopy-layer heat island effect in Athens.

When studying the canopy-layer UHI, attention should be paid to eliminate the unwanted effects of surface relief and elevation, otherwise the perceived "heat islands" may not be sufficiently urban-induced to warrant the use of this term (Stewart, 2011). Therefore, the current heat island analysis is based on comparing observations and model results between measurement sites that share similar topographic features. More precisely, three stations located in the Athens metropolitan area were selected as representative of urban conditions, namely stations 4, 6 and 15. These stations are located in "compact midrise" areas and show minor elevation variability (Table 1). Station 24 (Table 1), located in a "sparsely built" area outside the larger urban zone of the city, was chosen as representative of semi-rural conditions. The intensity of the UHI (UHII) was computed by subtracting the near-surface air temperature of station 24 from the spatially averaged temperature of stations 4, 6 and 15. The differences in elevation between the selected urban and semi-rural sites are below 40 m (Table 1), ensuring that the magnitude of the heat island cannot be misinterpreted.

Table 3 presents the measured and modeled UHII at 0800, 1400 and 2300 LT, for each of the two selected days. The urban/semi-rural temperature contrast is found to be diminished in the early morning, as expected by the quicker warming of the semi-rural site following sunrise (Bassara et al., 2008; Oke, 1982). The daytime UHII is simulated to be low, which is generally well expected (e.g. Memon et al., 2009), but its magnitude is underestimated. Last, the model manages to capture the formation of the nocturnal UHI, simulating higher nighttime temperatures for the urban sites than for the semi-rural site (Table 3).

Fig. 4 presents the observed and modeled diurnal course of the UHII, averaged over the two selected days. It can be seen that the model simulates the intensity of the UHI to be higher during the night (2100–0600 LT) than during the day (0700–2000 LT). This agrees well with both the ground-based measurements and earlier observational and/or numerical studies, reporting that the UHI is primarily a nocturnal effect (e.g. Bassara et al., 2008; Christen and Vogt, 2004; Giannaros and Melas, 2012; Miao et al., 2009; Papanastasiou and Kittas, 2011). Following sunrise (0700 LT), the UHII is successfully simulated to decrease abruptly. This is again a well known feature of the UHI diurnal cycle (e.g. Giannaros and Melas, 2012; Oke, 1987) that is mainly due to the reduced early morning heating rate of urban areas compared to their rural surroundings (Oke, 1982). However, the model does not manage to capture the formation of a weak urban cool island (UCI) during morning hours (0800–1100 LT). On the other hand, it seems able to simulate the formation of the nocturnal heat island in late afternoon hours (1800–1900 LT), an effect that can be attributed to the slowdown of the urban cooling rate (Oke, 1982).

4.3. Surface urban heat island

Fig. 5b and d presents the daytime and nighttime model simulated LST, respectively. As seen in Fig. 5b, the model simulates the

Table 3
Comparison between the observed and modeled UHI intensity at the designated times.

Date	UHI intensity (°C)					
	0800 LT		1400 LT		2300 LT	
	Observed	Modeled	Observed	Modeled	Observed	Modeled
July 24	0.17	−0.76	4.13	1.20	5.70	4.60
July 25	0.70	0.25	1.14	0.46	1.50	2.82

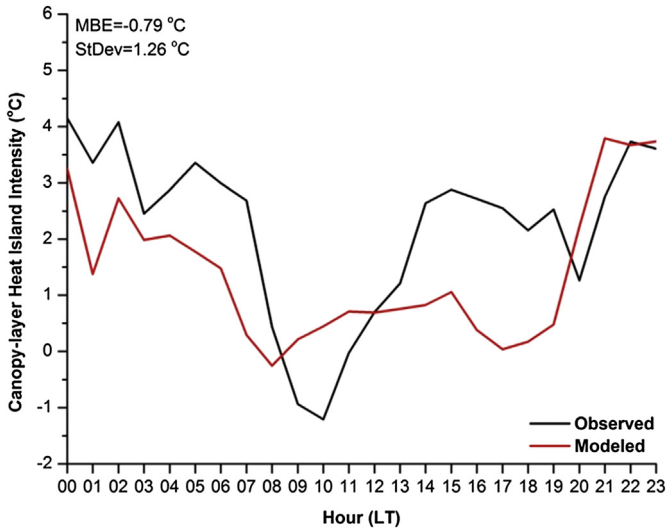

Fig. 4. Diurnal variation of the intensity of the UHI, averaged over the entire study time period.

existence of three daytime hot-spots, at Megara, Elefsina and Mesogeia Pl. (Fig. 1b), indicating that the center of Athens does not exhibit the highest LSTs. This particular effect is confirmed by the corresponding satellite-derived LST map (Fig. 5a), and is commonly referred to as the urban heat sink or negative heat island (Keramitsoglou et al., 2011). In the nighttime, the city centre is modeled to be warmer than its surroundings (Fig. 5d), as expected by the UHI phenomenon. The nighttime satellite image confirms this pattern (Fig. 5c), indicating however that the model overestimates the LST.

4.4. Land surface temperature assimilation

Fig. 6 summarizes the overall performance of the modeling system with ("assimilation") and without ("control") the ingestion of the satellite-retrieved LST data (see Section 3.3). The implementation of the LST assimilation scheme does not appear to have a clear impact on the overall model performance (Fig. 6a). Indeed, the changes in the frequencies of the various error classes do not exceed 1%, and thus they cannot be considered to be important. Further, the ingestion of the satellite-retrieved LST does not seem to induce significant changes in the model performance metrics over the considered LCZs (Fig. 6b).

Despite the apparently discouraging preliminary results, it cannot be yet claimed that the implementation of the assimilation scheme does not have any impact on model performance. The ingestion of the LST data does have an effect on model performance, inducing changes in the model biases that can be as high as 0.2 °C (Fig. 7). This can be more clearly seen during the first 4–5 h of the simulation. Thereafter, the positive (bias reduction) impact declines and even turns negative, increasing model biases (e.g.

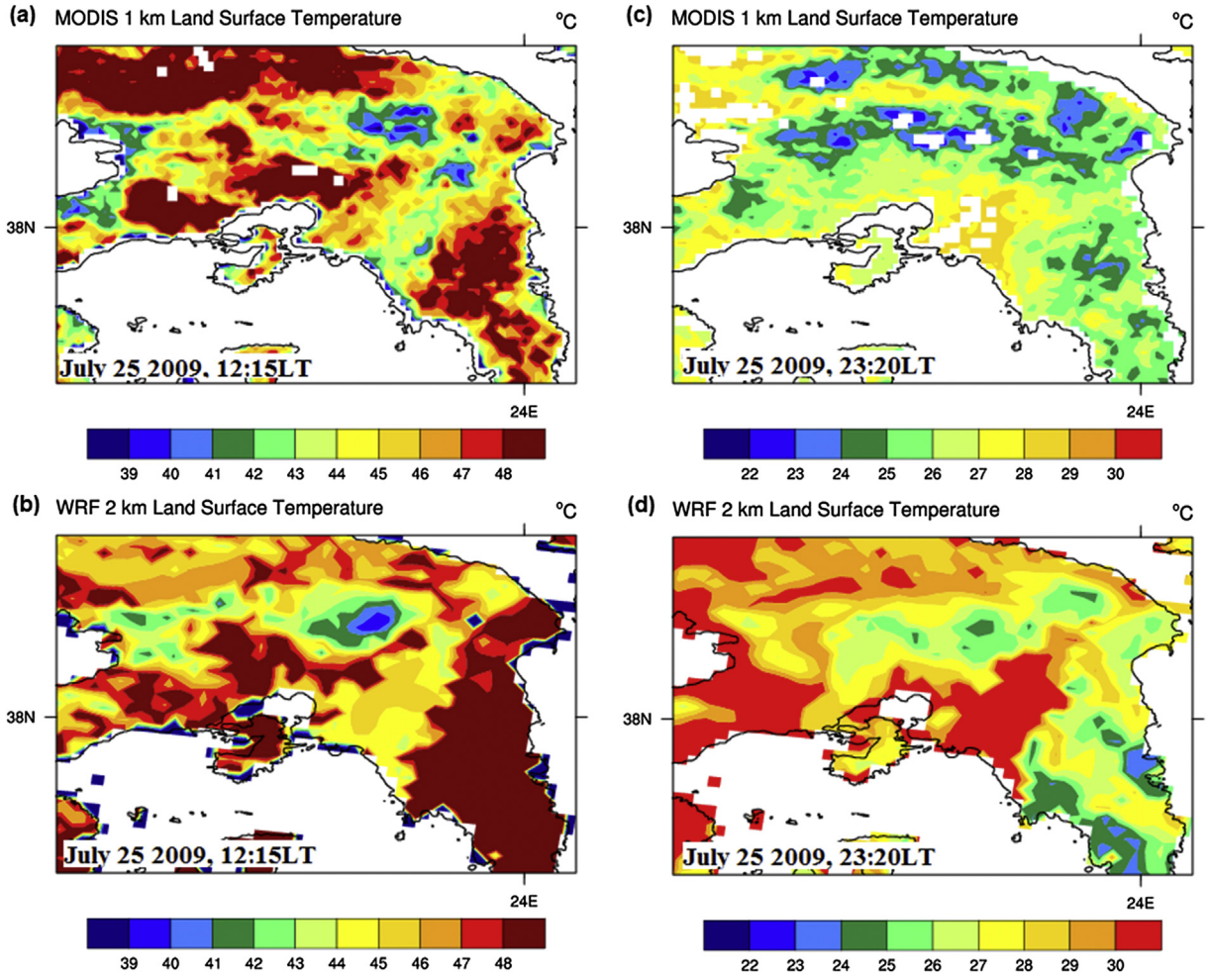

Fig. 5. Observed (a,c) and modeled (b,d) spatial variation of the land surface temperature on July 25, 2009 at 1215 LT and 2320 LT (Source of satellite LST maps: UHI project).

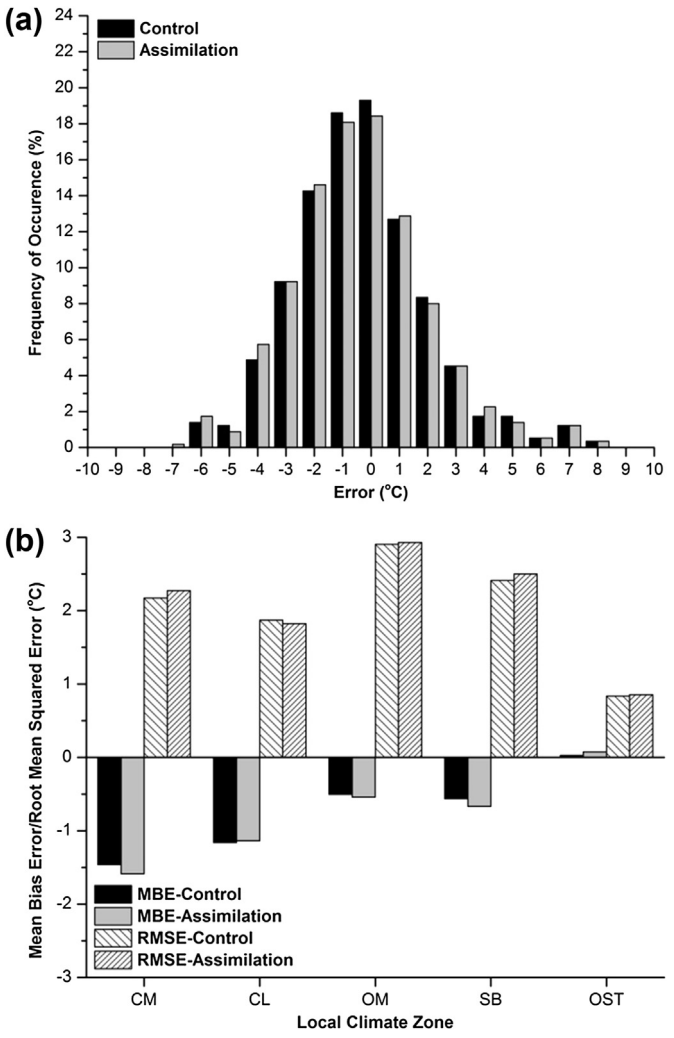

Fig. 6. (a) Error distribution (model minus observations) of the modeled near-surface air temperature over all measurement sites. (b) Model performance metrics (MBE, RMSE) for the near-surface air temperature, grouped by local climate zone.

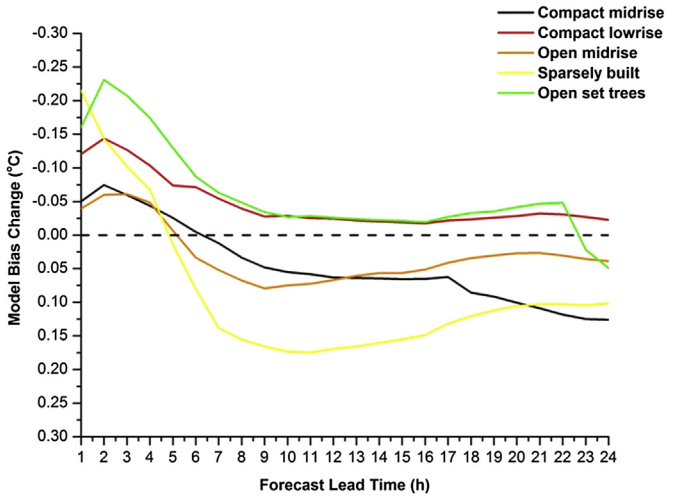

Fig. 7. Change in the model bias (bias after minus bias before the assimilation) as a function of the forecast lead time (hours since 1200 UTC July 24, 2009), grouped by local climate zone.

"sparsely built" sites, Fig. 7). Therefore, the implementation of the assimilation scheme appears to have a short-term impact on improving the modeling system's near-surface air temperature estimates. This impact is more evident during the first few hours (4–5 h) of the simulation that follow the ingestion of the LST data. This finding provides indications that a continuous implementation of the assimilation scheme (e.g. every 3–6 h) could possibly result to more significant improvements in the model performance.

5. Conclusions

In the present study, the coupled WRF/Noah modeling system was implemented over the city of Athens, Greece, for studying the UHI effect, both in the canopy-layer and the surface. Additionally, a simple data assimilation scheme for satellite-retrieved LST was tested. The performance of the modeling system was evaluated during two selected dates, using a subset of the observational data collected during the THERMOPOLIS2009 campaign.

Comparisons made with observations demonstrated reasonably successful simulations of the major features of the UHI effect, indicating the overall suitability of the WRF/Noah modeling system for studying this particular phenomenon. The conducted analysis suggests the following:

1) The city of Athens is characterized by a rather strong UHI effect (>4 °C) during the night, whereas in early morning and solar peak hours the thermal contrast is less pronounced.
2) The mean diurnal course of the Athens' heat island agrees well with the theory of UHI formation (Oke, 1982); the UHI is found to be more pronounced during the night, decreasing abruptly following sunrise and intensifying following sunset.
3) During the day, the city surface acts as an urban heat sink (Keramitsoglou et al., 2011). Conversely, the city surface appears to be warmer than its surroundings during the night.

The LST data assimilation experiment provided indications of a small impact on model performance. The ingestion of the satellite-retrieved LST data into the meteorological model reduced slightly the model's temperature biases, in particular during the first few hours following the assimilation. The short-term duration of the positive impact could be possibly because only one LST image was assimilated due to limited data availability at the required time scale. However, the preliminary conclusions suggest that the assimilation scheme should be further tested and evaluated.

Acknowledgments

The present work was conducted in the frame of the "Urban Heat Islands and Urban Thermography" project, funded by the European Space Agency (ESA) (Contract No. 21913/08/I-LG). Observational data used in the present study were acquired during the THERMOPOLIS2009 campaign, funded by ESA (Contract No. 22693/09/I-EC).

References

Bassara, J.P., Hall Jr., P.K., Schroeder, A.J., Illston, B.G., Nemunaities, K.L., 2008. Diurnal cycle of the Oklahoma City urban heat island. Journal of Geophysical Research 113, 1–16.

Bosilovich, M., Radakovich, J., da Silva, A., Todling, R., Verter, F., 2007. Skin temperature analysis and bias correction in a coupled land-atmosphere data assimilation system. Journal of the Meteorological Society of Japan 85A, 205–228.

Chen, F., Dudhia, J., 2001. Coupling an advanced land surface-hydrology model with the Penn State-NCAR MM5 modeling system. Part I: model implementation and sensitivity. Monthly Weather Review 129, 569–585.

Chen, F., Mitchell, K., Schaake, J., Xue, Y., Pan, H.L., Koren, V., Duan, Q.Y., Ek, M., Betts, A., 1996. Modeling of land surface evaporation by four schemes and comparison with FIFE observations. Journal of Geophysical Research 101 (D3), 7251–7268.

Christen, A., Vogt, R., 2004. Energy and radiation balance of a central European city. International Journal of Climatology 24, 1395–1421.

Conti, S., Meli, P., Mineli, G., Solimini, R., Toccaceli, V., Vichi, M., Beltrano, C., Perini, L., 2005. Epidemiologic study of mortality during the summer 2003 heat wave in Italy. Environmental Research 98, 390–399.

Daglis, I.A., Keramitsoglou, I., Amiridis, V., Petropoulos, G., Melas, D., Giannaros, T., Kourtidis, K., Sobrino, J.A., Manunta, P., Gröbner, J., Paganini, M., Bianchi, R., 2010a. Investigating the urban heat island (UHI) effect in Athens through a combination of space, airborne and ground-based observations. In: Argyriou, A.A., Kazantzidis, A.J. (Eds.), Proceedings of COMECAP 2010 (Conference on Meteorology, Climatology and Atmospheric Physics 2010). University of Patras.

Daglis, I.A., Rapsomanikis, S., Kourtidis, K., Melas, D., Papayannis, A., Keramitsoglou, I., Giannaros, T., Amiridis, V., Petropoulos, G., Georgoulias, A., Sobrino, J.A., Manunta, P., Gröbner, J., Paganini, M., Bianchi, R., 2010b. Results of the DUE THERMOPOLIS campaign with regards to the urban heat island (UHI) effect in Athens. ESA SP-686. In: Proceedings of the ESA Living Planet Symposium 2010. European Space Agency.

Dandou, A., Tombrou, M., Akylas, E., Soulakellis, N., Bossioli, E., 2005. Development and evaluation of an urban parameterization scheme in the Penn State/NCAR Mesoscale Model (MM5). Journal of Geophysical Research 110, D10102.

Dandou, A., Tombrou, M., Soulakellis, N., 2009. The influence of the city of Athens on the evolution of the sea-breeze front. Boundary-Layer Meteorology 131, 35–51.

Dudhia, J., 1989. Numerical study of convection observed during the winter monsoon experiment using a mesoscale two-dimensional model. Journal of Atmospheric Sciences 46, 3077–3107.

Dudhia, J., Hong, S.Y., Lim, K.S., 2008. A new method for representing mixed-phase particle fall speeds in bulk microphysics parameterizations. Journal of the Meteorological Society of Japan 86A, 33–44.

Ferretti, R., Mastrantonio, G., Argentini, S., Santoleri, R., Viola, A., 2003. A model-aided investigation of winter thermally driven circulation on the Italian Tyrrhenian coast: a case study. Journal of Geophysical Research 108 (D24), 4777.

Giannaros, T.M., Melas, D., 2012. Study of the urban heat island in a coastal Mediterranean city: the case study of Thessaloniki, Greece. Atmospheric Research 118, 103–120.

Grimmond, C.S.B., Oke, T.R., 1995. Comparison of heat fluxes from summertime observations in the suburbs of four North American cities. Journal of Applied Meteorology 34, 873–889.

Grossi, P., Thunis, P., Martilli, A., Clappier, A., 2000. Effect of sea breeze on air pollution in the Greater Athens area. Part II: analysis of different emission scenarios. Journal of Applied Meteorology 39, 563–575.

Hong, S.Y., Dudhia, J., Chen, S.H., 2004. A revised approach to ice microphysical processes for the bulk parameterization of clouds and precipitation. Monthly Weather Review 132, 103–120.

Hong, S.Y., Noh, Y., Dudhia, J., 2006. A new vertical diffusion package with an explicit treatment of entrainment processes. Monthly Weather Review 134, 2318–2341.

Houghton, J.T., Ding, Y., Griggs, D.J., Noguer, M., van der Linden, P.J., Dai, X., Mashell, K., Johnson, C. (Eds.), 2001. Climate Change 2001: The Scientific Basis. Cambridge University Press, Cambridge, 881 pp.

Jacquenim, B., Noilhan, J., 1990. Sensitivity study and validation of a land surface parameterization using the HAPEX-MOBILHY data set. Boundary-Layer Meteorology 52, 92–134.

Jimenez-Munoz, J.C., Sobrino, J.A., 2008. Split-window coefficients for land surface temperature retrieval from low-resolution thermal infrared sensors. IEEE Geoscience and Remote Sensing Letters 5 (4), 806–809.

Kain, J.S., 2004. The Kain–Fritsch convective parameterization: an update. Journal of Applied Meteorology 43, 170–181.

Kanda, M., Kawai, T., Kanega, M., Moriwaki, R., Narita, K., Hagishima, A., 2005. A simple energy balance model for regular building arrays. Boundary-Layer Meteorology 116, 423–443.

Katsoulis, B.D., 1987. Indications of change of climate from the analysis of air temperature time series in Athens, Greece. Climatic Change 10, 67–79.

Keramitsoglou, I., Kiranoudis, C.T., Ceriola, G., Weng, Q., Rajasekar, U., 2011. Identification and analysis of urban surface temperature patterns in Greater Athens, Greece, using MODIS imagery. Remote Sensing of Environment 115, 3080–3090.

Konopacki, S., Akbari, H., 2002. Energy Savings for Heat Island Reduction Strategies in Chicago and Houston (Including Updates for Baton Rouge, Sacramento, and Salt Lake City). Draft Final Report, LBNL-49638. University of California, Berkeley.

Koren, V., Schaake, J., Mitchell, K., Duan, Q.Y., Chen, F., Bake, J.M., 1999. A parameterization of snowpack and frozen ground intended for NCEP weather and climate models. Journal of Geophysical Research 104 (D16), 19569–19585.

Kotroni, V., Kallos, G., Lagouvardos, K., Varinou, M., Walko, R., 1999. Numerical simulation of the meteorological and dispersion conditions during an air pollution episode over Athens, Greece. Journal of Applied Meteorology 38, 432–447.

Kusaka, H., Kondo, H., Kikegawa, Y., Kimura, F., 2001. A simple single-layer urban canopy model for atmospheric models: comparison with multi-layer and slab models. Boundary-Layer Meteorology 101, 329–358.

Kusaka, H., Chen, F., Tewari, M., Dudhia, J., Gill, D.O., Duda, M.G., Wang, W., 2012. Numerical simulation of urban heat island effect by the WRF model with 4-km grid increment: an inter-comparison study between the urban canopy model and slab model. Journal of the Meteorological Society of Japan 90B, 33–45.

Lakshmi, V., 2000. A simple surface temperature assimilation scheme for use in land surface models. Water Resources Research 36, 3687–3700.

Lin, Y.L., Farley, R.D., Orville, H.D., 1983. Bulk parameterization of the snow field in a cloud model. Journal of Applied Meteorology 22, 1065–1092.

Liu, Y., Chen, F., Warner, T., Bassara, J., 2006. Verification of a mesoscale data-assimilation and forecasting system for the Oklahoma City area during the Joint Urban 2003 field project. Journal of Applied Meteorology and Climatology 45, 912–929.

Mahrt, L., Ek, M., 1984. The influence of atmospheric stability on potential evaporation. Journal of Applied Meteorology 23, 222–234.

Mahrt, L., Pan, H.L., 1984. A two-layer model for soil hydrology. Boundary-Layer Meteorology 29, 1–20.

Martilli, A., 2007. Current research and future challenges in urban mesoscale modeling. International Journal of Climatology 27, 1909–1918.

Martilli, A., Roulet, Y.A., Junier, M., Kirchner, F., Rotach, M.W., Clappier, A., 2003. On the impact of urban surface exchange parameterizations on air quality simulations: the Athens case. Atmospheric Environment 37, 4217–4231.

Masson, V., 2006. Urban surface modeling and the meso-scale impact of cities. Theoretical and Applied Climatology 84, 35–45.

Melas, D., Ziomas, I., Klemm, O., Zerefos, C., 1998a. Anatomy of sea breeze circulation in greater Athens under weak large-scale ambient winds. Atmospheric Environment 32, 2223–2237.

Melas, D., Ziomas, I., Klemm, O., Zerefos, C., 1998b. Flow dynamics in greater Athens under moderate large-scale flow. Atmospheric Environment 32, 2209–2222.

Memon, R.A., Leung, D.Y.C., Liu, C.-H., 2009. An investigation of urban heat island intensity (UHII) as an indicator of urban heating. Atmospheric Research 94, 491–500.

Miao, J.F., Chen, D., Borne, K., 2007. Evaluation and comparison of Noah and Pleim-Xiu land surface models in MM5 using GOTE2001 data: spatial and temporal variations in near-surface air temperature. Journal of Applied Meteorology and Climatology 46, 1587–1605.

Miao, S., Chen, F., LeMone, A.M., Tewari, M., Li, Q., Wang, Y., 2009. An observational and modelling study of characteristics of urban heat island and boundary layer structures in Beijing. Journal of Applied Meteorology and Climatology 48, 484–501.

Moussiopoulos, N., Sahm, P., Kessler, C., 1995. Numerical simulation of photochemical smog formation in Athens, Greece – a case study. Atmospheric Environment 29, 3619–3632.

Oke, T.R., 1982. The energetic basis of the urban heat island. Quarterly Journal of the Royal Meteorological Society 108, 1–24.

Oke, T.R., 1987. Boundary Layer Climates, second ed. Routledge and John Wiley and Sons, 435 pp.

Pal, S., Xueref-Remy, I., Ammoura, L., Chazette, P., Gibert, F., Royer, P., Dieudonné, E., Dupont, J.C., Haeffelin, M., Lac, C., Lopez, M., Morille, Y., Ravetta, F., 2012. Spatio-temporal variability of the atmospheric boundary layer depth over the Paris agglomeration: an assessment of the impact of the urban heat island intensity. Atmospheric Environment 63, 261–275.

Pan, H.L., Mahrt, L., 1987. Interaction between soil hydrology and boundary-layer development. Boundary-Layer Meteorology 38, 185–202.

Papanastasiou, D., Kittas, C., 2011. Maximum urban heat island intensity in a medium-sized coastal Mediterranean city. Theoretical and Applied Climatology 107, 407–416.

Rosenfeld, A.H., Akbari, H., Romn, J.J., Pomerantz, M., 1998. Cool communities: strategies for heat island mitigation and smog reduction. Energy and Buildings 28, 51–62.

Salamanca, F., Martilli, A., Yague, C., 2011. A numerical study of the urban heat island over Madrid during the DESIREX (2008) campaign with WRF and an evaluation of simple mitigation strategies. International Journal of Climatology 32, 2372–2386.

Schwarzkopf, M.D., Fels, S.B., 1991. The simplified exchange method revisited – an accurate, rapid method for computation of infrared cooling rates and fluxes. Journal of Geophysical Research 96 (D5), 9075–9096.

Skamarock, W.C., Klemp, J.B., Dudhia, J., Gill, D.O., Barker, D.M., Duda, M.G., Huang, X.Y., Wang, W., Powers, J.G., 2008. A Description of the Advanced Researcher WRF Version 3. NCAR Technical Note, NCAR/TN-475 + STR, June 2008, Boulder, Colorado, USA, 125 pp.

Stewart, I.D., 2011. A systematic review and scientific critique of methodology in modern urban heat island literature. International Journal of Climatology 31, 200–217.

Stewart, I.D., Oke, T.R., 2009a. Conference notebook – a new classification system for urban climate sites. Bulletin of the American Meteorological Society 90, 922–923.

Stewart, I.D., Oke, T.R., 2009b. Classifying urban climate field sites by "local climate zones": the case of Nagano, Japan. Preprints, Seventh International Conference on Urban Climate, June 29–July 3 2009, Yokohama, Japan.

Van Wevenberg, K., De Ridder, K., Van Rompaey, A., 2008. Modeling the contribution of the Brussels heat island to a long temperature time series. Journal of Applied Meteorology and Climatology 47, 976–990.

Zhang, J., Zhang, X., 2010. A soil moisture assimilation scheme using satellite-retrieved skin temperature in meso-scale weather forecast model. Atmospheric Research 95, 333–352.